Received: 14 April 2018 | Revised: 24 December 2018 | Accepted: 6 March 2019

DOI: 10.1002/eqe.3173

RESEARCH ARTICLE

WILEY

The effect of amplitude scaling limits on conditional spectrum-based ground motion selection

Wenqi Du[1] | Chao-Lie Ning[2] | Gang Wang[3]

[1]State Key Laboratory of Water Resources and Hydropower Engineering Science, Institute of Engineering Risk and Disaster Prevention, Wuhan University, Wuhan, China

[2]Shanghai Institute of Disaster Prevention and Relief, Tongji University, Shanghai, China

[3]Department of Civil and Environmental Engineering, Hong Kong University of Science and Technology, Hong Kong SAR

Correspondence
Wenqi Du, State Key Laboratory of Water Resources and Hydropower Engineering Science, Institute of Engineering Risk and Disaster Prevention, Wuhan University, 299 Bayi Road, Wuhan 430072, China.
Email: wqdu@ntu.edu.sg

Funding information
Hong Kong Research Grants Council, Grant/Award Number: 16204618; National Natural Science Foundation of China, Grant/Award Number: 51828902

Summary

Amplitude scaling is commonly used to select ground motions matching a target response spectrum. In this paper, the effect of scaling limits on ground motion selection, based on the conditional spectrum framework, is investigated. Target spectra are computed for four probabilistic seismic hazard cases in Western United States, and 16 ground motion suites are selected using different scaling limits (ie, 2, 5, 10, and 15). Comparison of spectral acceleration distributions of the selected ground motion suites demonstrates that the use of a scaling limit of 2 yields a relatively poor representation of the target spectra, because of the small limit leading to an insufficient number of available ground motions. It is also shown that increasing scaling limit results in selected ground motions with generally increased distributions of Arias intensity and significant duration $Ds_{5\text{-}75}$, implying that scaling limit consideration can significantly influence the cumulative and duration characteristics of selected ground motions. The ground motion suites selected are then used as input for slope displacement and structural dynamic analyses. Comparative results demonstrate that the consideration of scaling limits in ground motion selection has a notable influence on the distribution of the engineering demand parameters calculated (ie, slope displacement and interstory drift ratio). Finally, based on extensive analyses, a scaling limit range of 3 to 5 is recommended for general use when selecting ground motion records from the NGA-West2 database.

KEYWORDS

conditional spectrum, generalized IMs, ground motion selection, scaling limit, seismic dynamic analysis

1 | INTRODUCTION

Dynamic time history analysis is usually required in modern design codes,[1,2] and a suite of ground motions that match a target response spectrum are needed as input. The conditional mean spectrum,[3] conditional spectrum (CS),[4] and the commonly used uniform hazard spectrum can be regarded as the "target" in engineering practice. Thus, selecting a suite of appropriate ground motion records plays an important role in assessing the dynamic response of structures or infrastructures. Many methods and tools have been developed in selecting ground motions to date.[3-15] Classic methods are conducted to select ground motions that have response spectra matching the specified target (mean) spectrum only,[3,6,14]

while advanced methods have been proposed to select ground motions matching both the mean and variance of the target spectrum, such as the CS-based ground motion selection approach.[4,11] To further quantify the distribution of multiple intensity measures (IMs) rather than spectral acceleration (SA) ordinates only, Tarbali and Bradley[13] presented a ground motion selection algorithm based on the generalized conditional IM (GCIM) methodology.[7] More recently, Du and Wang[15] demonstrated the advantage of using generalized IMs as "target" in selecting ground motions for engineering applications.

Because of the scarcity of high-amplitude ground motion records, selecting and scaling ground motions to reach the target spectrum level are then a procedure commonly used for dynamic analysis.[16-18] Despite its prevalent use, such ground motion scaling is just an empirical approach without a physical premise. Some researchers have stated that (large) scaling of ground motions may result in a bias in the response of nonlinear engineering systems.[19-21] Yet, in the earthquake engineering community, there is currently no consensus about the impact of using scaled ground motions in dynamic analysis, as well as the "appropriate" scaling limit in selecting ground motions. Such limit is usually subjective, with scaling bounds ranging from 1 (no scaling allowed) to more than 10 in different applications. Specifically, although amplitude scaling is generally recommended in recent ground motion selection approaches,[4,9] no guidance or recommendation exists on how to specify an appropriate scaling limit.

The objective of this paper is thus to quantify the influence of scaling limit on ground motion selection based on the CS-based methodology. Four scaling limits (ie, 2, 5, 10, and 15) are considered to select ground motions for four seismic hazard cases. The representative seismic hazard cases, along with the ground motion dataset employed, are introduced in Section 2. The characteristics of ground motion suites selected using different scaling limits are presented and compared in Section 3. In Sections 4 and 5, seismic slope displacement and structural analyses are carried out using the selected ground motion suites, and the influence of scaling limits on the dynamic performance of the engineering systems is scrutinized. Finally, general recommendations and concluding remarks are provided in Sections 6 and 7, respectively.

2 | SEISMIC HAZARD ANALYSIS AND GROUND MOTION DATASET

2.1 | Representative seismic hazard cases

The standard procedures for specifying a target CS are listed as follows: (a) Probabilistic seismic hazard analysis (PSHA) is conducted at a given site for a period of interest T^*; (b) the distribution of causal parameters (eg, moment magnitude M_w and rupture distance R_{rup}) contributing to the occurrence of a specified hazard level is then obtained by deaggregation; (c) a CS (both mean and variance) can be calculated based on a combination of deaggregation results, ground motion prediction equations (GMPEs), and empirical correlations between pairs of SAs.[22] The detailed procedures can be found in Baker.[3]

Four seismic hazard cases are considered in this paper, including two sites (San Francisco and Seattle) in Western United States, each with two SA periods of interest (conditioning period T^* as 0.2 and 1.0 s, respectively). The detailed information about the hazard cases, including its geographic location, site condition, conditioning period, and hazard level, is listed in Table 1. The PSHA and deaggregation results were obtained from the United States Geological Survey (USGS) Web tool.[23] Figure 1 illustrates the deaggregation distributions of M_w, R_{rup}, and ε for hazard cases I and IV, respectively. It can be seen that for case I, the near-fault earthquake scenarios contribute predominantly to the occurrence of the hazard, while for case IV, both near-fault and moderate-to-far distance scenarios have a contribution to the occurrence of the hazard level. Therefore, the four seismic hazard cases considered cover a relatively wide range of earthquake scenarios.

TABLE 1 Summary of the seismic hazard cases considered in this study

Case	Site	Latitude, °	Longitude, °	V_{s30}, m/s	Conditioning Period, s	Hazard Level
I	San Francisco	37.775	−122.419	360	0.2	2% in 50 y
II	San Francisco	37.775	−122.419	360	1.0	2% in 50 y
III	Seattle	47.606	−122.332	360	0.2	2% in 50 y
IV	Seattle	47.606	−122.332	360	1.0	2% in 50 y

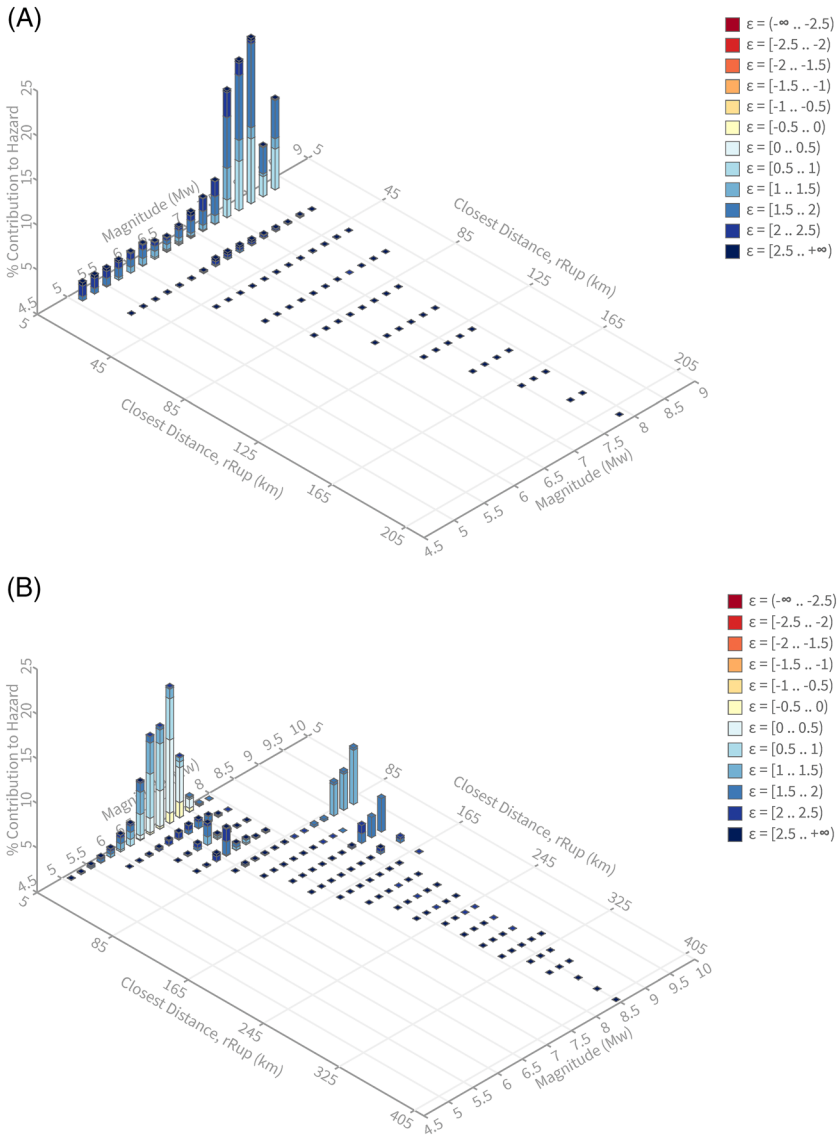

FIGURE 1 Probabilistic seismic hazard analysis deaggregation distributions for a 2% exceedance probability in 50 years for (A) case I: San Francisco at spectral acceleration (SA) at 0.2 s hazard; (B) case IV: Seattle at SA (1 s) hazard. Figures were obtained from the United States Geological Survey (USGS) interactive Web tool.[23] The mean deaggregation results are listed in Table 2 [Colour figure can be viewed at wileyonlinelibrary.com]

The mean values of M_w/R_{rup} from deaggregation results (denoted as $\overline{M}_w$ and $\overline{R}_{rup}$ hereafter) for the four hazard cases are listed in Table 2. It is worth noting that the $\overline{M}_w$ and $\overline{R}_{rup}$ values for cases III and IV are approximations of the deaggregation results, because of multiple seismic sources contributing to their seismic hazard (Figure 1B). For each hazard case, the GMPE-specific ε value, which is the number of standard deviations by which the target SA is larger than the predicted median,[24] is calculated and listed in Table 2. Therefore, the $\overline{M}_w/\overline{R}_{rup}/\varepsilon$ values represent the controlling earthquake scenario regarding the target hazard level of each case. We do not specify a selection constraint on M_w and R_{rup}, because it would have a similar effect as scaling limit in the selection process. Besides, to select a suite of ground motions with similar site characteristics, a selection constraint on V_{s30} (time-averaged shear wave velocity in

TABLE 2 Representative hazard targets based on deaggregation results and selection constraints assigned in ground motion selection

Hazard Case	Target				Selection Constraint	
	$\overline{M}_w$	$\overline{R}_{rup}$, km	V_{s30}, m/s	ε	$V_{s30,\ min}$, m/s	$V_{s30,\ max}$, m/s
I	7.36	13.71	360	2.53	180	540
II	7.7	13.95	360	1.66	180	540
III	7.01	38.09	360	3.40	180	540
IV	7.43	37.7	360	2.34	180	540

the upper 30 m of a soil profile) suggested by Tarbali and Bradley[25] is adopted. As shown in Table 2, only records with V_{s30} between 0.5 and 1.5 times the site V_{s30} value are considered as candidate ground motions.

2.2 | Ground motion dataset

A subset of the Pacific Earthquake Engineering Research Center's NGA-West2 database[26] is utilized in this study. The whole NGA-West2 database includes 21 533 three-component uniformly processed recordings from 599 shallow crustal earthquake events. Following the selection criteria adopted by Campbell and Bozorgnia,[27] some low-quality, incomplete, unreliable, or non–free-field recordings are removed from the original database. Ground motions that fail to satisfy the selection criteria on V_{s30} are further excluded. The reduced dataset contains 10 679 recordings from 310 earthquakes, with M_w ranging from 3.05 to 7.9 and R_{rup} ranging from 0.1 to 499.54 km. Figure 2 shows the moment magnitude and rupture distance distribution of the final dataset. Note that only the two horizontal components of ground motion recordings are used in this study.

3 | INFLUENCE OF SCALING LIMITS ON CHARACTERISTICS OF SELECTED GROUND MOTIONS

3.1 | Various limits of ground motion scaling

In this section, the CS-based ground motion selection is conducted for the four target hazard cases, and suites of ground motions are selected using various scaling limits. The scale factor groups considered are listed in Table 3, where groups A and D represent the use of the narrowest and widest range of scale factors, respectively. For each target case and

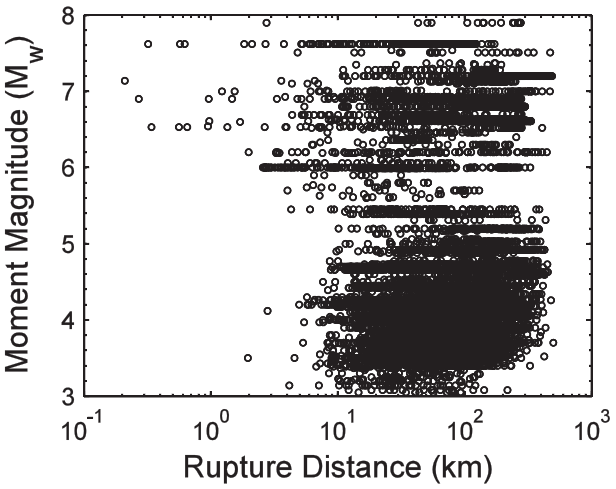

FIGURE 2 Distribution of moment magnitude versus rupture distance for earthquake ground motions selected from the NGA-West2 database

TABLE 3 Number of available ground motion recordings for each hazard case and scaling limit assigned

		Scale Factor Groups			
		A	B	C	D
No. of Usable Records		0-2	0-5	0-10	0-15
Hazard Cases	I	60	397	860	1233
	II	62	325	708	1015
	III	113	530	1037	1470
	IV	138	552	1026	1306

scaling limit, the number of available ground motions in the dataset is also listed in Table 3. As expected, the number of available ground motions increases as scaling limit increases.

3.2 | Ground motion selection approach

The CS provides the statistical distribution of SA ordinates that are conditioned on a target value at T^*. The conditional mean and standard deviation for logarithmic SA_i (SA value at a specified period i) can be estimated as[3]

$$\mu_{\ln SA_i|\ln SA(T^*)} = \mu_{\ln SA_i}(M_w, R_{rup}, \theta) + \sigma_{\ln SA_i}(M_w, R_{rup}, \theta)\cdot\rho_{\ln SA_i, \ln SA(T^*)}\cdot\varepsilon(T^*), \tag{1}$$

$$\sigma_{\ln SA_i|\ln SA(T^*)} = \sigma_{\ln SA_i}(M_w, R_{rup}, \theta)\cdot\sqrt{1-\rho^2_{\ln SA_i, \ln SA(T^*)}}, \tag{2}$$

where $\mu_{\ln SA_i}(M_w, R_{rup}, \theta)$ and $\sigma_{\ln SA_i}(M_w, R_{rup}, \theta)$ denote the predicted median and standard deviation for SA_i under a specified earthquake scenario (M_w, R_{rup}, θ); $\rho_{\ln SA_i, \ln SA(T^*)}$ is the correlation coefficient between SA_i and $SA(T^*)$; and $\varepsilon(T^*)$ is the number of standard deviations to quantify the difference between the target $\ln SA(T^*)$ and the predicted median $\mu_{\ln SA_i}(M_w, R_{rup}, \theta)$.

The selection algorithm proposed by Jayaram et al[4] was adopted to select ground motions. The "target" consists of SA ordinates at 24 periods over the whole period range (T = 0.01, 0.02, 0.05, 0.1, 0.125, 0.15, 0.2, 0.25, 0.3, 0.4, 0.5, 0.7, 0.9, 1.0, 1.2, 1.4, 1.7, 2.0, 2.5, 3.0, 4.0, 5.0, 7.5, 10.0 s). The NGA-West2 GMPE proposed by Campbell and Bozorgnia[27] was utilized for predicting the (unconditional) distribution of SAs. The empirical correlation model proposed by Jayaram and Baker[22] was used to construct the covariance matrix between SAs. The number of ground motion recordings selected (sample size) in each suite is set as 30. To refine the ground motion suite selected, it is desirable to repeat the selection process for several times. This is called a replicate selection procedure.[13,15] The number of replicate selections is set as 4 herein. The greedy optimization technique introduced by Jayaram et al[4] was also used to minimize the mismatch between ground motion ensembles and the "target".

A global residual R, which quantifies the difference between the statistical distribution of the selected ground motion suite and the prescribed target distribution,[9,15] is defined as

$$R = \sum_{i=1}^{N_{SA}} \left[w_i\left(\hat{m}_{\ln SA_i} - \mu_{\ln SA_i}\right)^2 + w_i\left(\hat{s}_{\ln SA_i} - \sigma_{\ln SA_i}\right)^2 \right], \tag{3}$$

where $\hat{m}_{\ln SA_i}$ and $\hat{s}_{\ln SA_i}$ are the sample mean and standard deviation of $\ln SA_i$ of the selected ground motion suite, respectively; $\mu_{\ln SA_i}$ and $\sigma_{\ln SA_i}$ denote the target mean and standard deviation calculated based on Equations (1) and (2); and w_i is the assigned weight to SA_i. Among the replicate selections, the ground motion suite that minimizes R is selected as the final suite, which consists of 30 acceleration-time series. Thus, R can be used to compare the appropriateness of the ground motion suites selected using different scaling limits. Note that equal weight w is assigned to the SA ordinates considered in this study.

3.3 | Comparison of SA distributions of the selected ground motion suites

Following the procedures introduced above, 16 ground motion suites were selected to match the target spectra of the seismic hazard cases. Figures 3 and 4 display the response spectra of ground motion suites selected using various scaling limits (groups A-D) for hazard cases I and IV, respectively. The statistical distributions (median, 2.5th and 97.5th percentiles) of the SA ordinates of selected ground motions are also compared with the "target" in each plot. It is observed that the statistical distributions of the selected ground motion suites generally resemble the prescribed target distributions, indicating the robustness of the ground motion selection approach. Besides, the misfit of ground motions selected based on the smallest scaling limit (group A) is more noticeable than those of the other groups (especially in Figure 4). This is not a surprise because of the much fewer available ground motions in such a scaling limit (as listed in Table 3). Figure 5A,B shows the cumulative distribution functions (CDFs) of scale factors utilized in hazard cases I and IV, respectively. As expected, a larger scaling limit (eg, group D) leads to a wider distribution of scale factors. It is worth noting that, although not illustrated in this manuscript, similar observations are also made for hazard cases II and III.

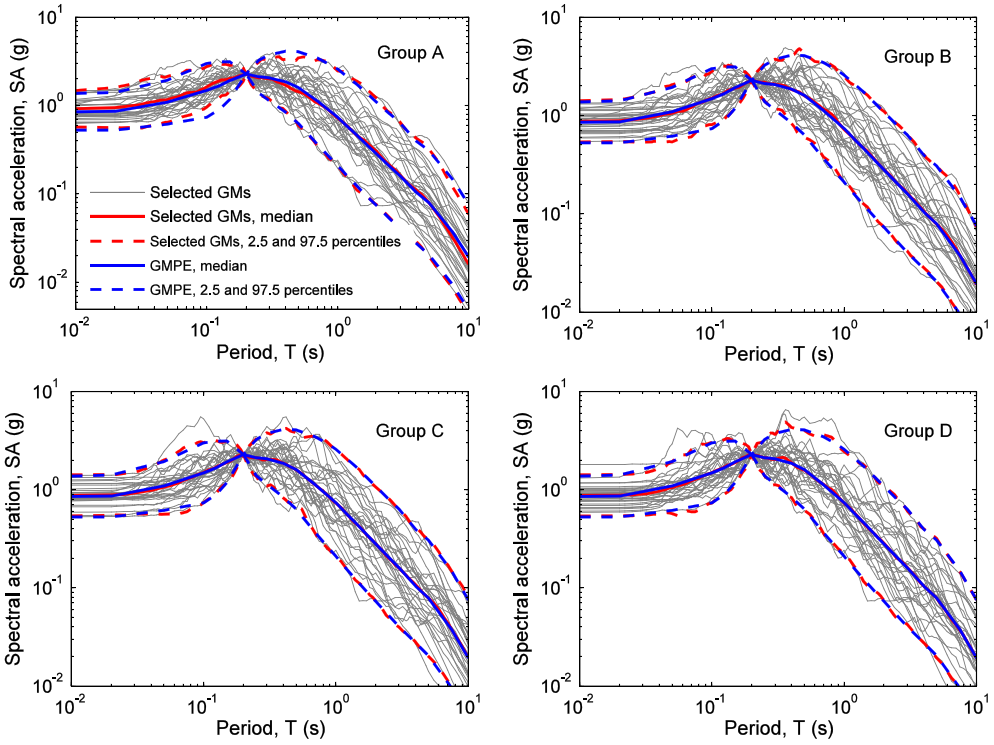

FIGURE 3 Spectral distributions of the selected ground motions considering different scaling limits (groups A-D) for seismic hazard case I (T^* = 0.2 s, 2% in 50-y hazard level in San Francisco)

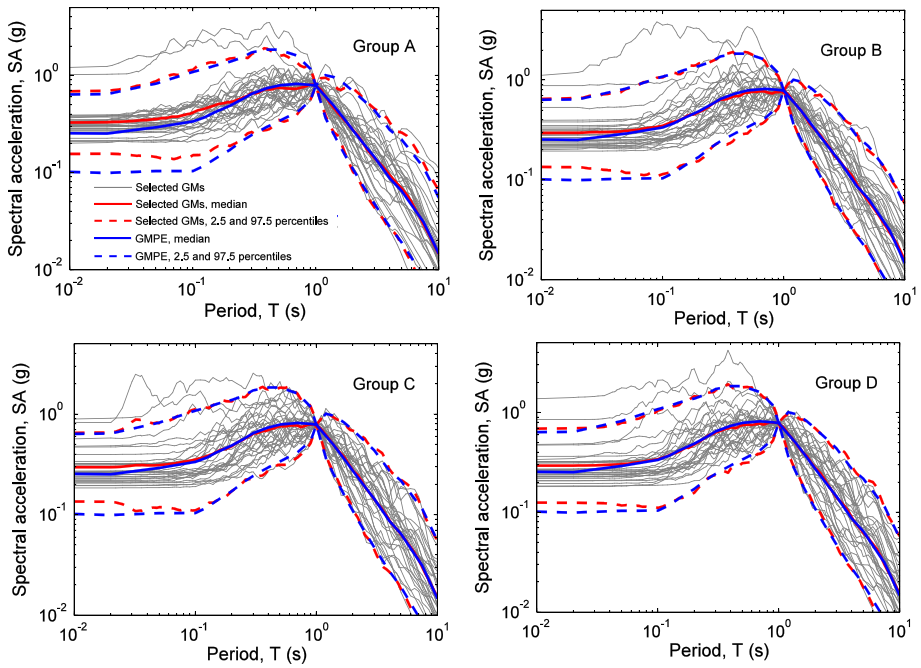

FIGURE 4 Spectral distributions of the selected ground motions considering different scaling limits (groups A-D) for hazard case IV (T^* = 1 s, 2% in 50-y hazard level in Seattle). The calculated global residuals R for groups A to D are 0.40, 0.10, 0.09, and 0.07, respectively

Figure 6 summarizes the calculated global residuals R for ground motion suites selected using various scaling limits for all seismic hazard cases. Two observations can be made from this figure. First, as noted above, the use of the smallest scaling limit (group A) yields the largest R, as a result of the fewest number of available ground motions. Second, although the use of an excessive scaling limit (ie, groups C and D) brings in a great number of available ground motions,

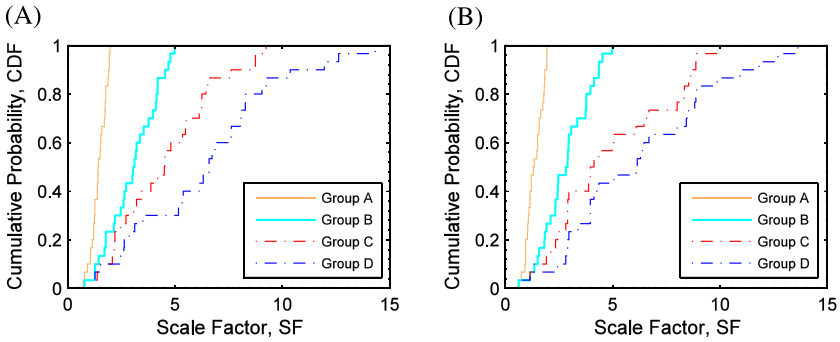

FIGURE 5 Distribution of scale factors employed for the selected ground motion suites for (A) case I and (B) case IV, respectively

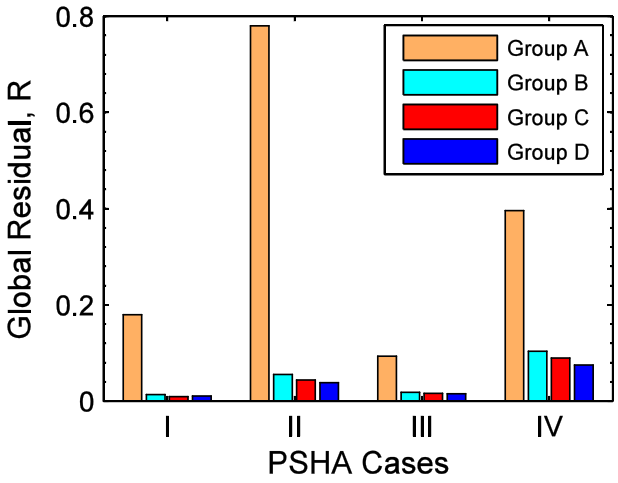

FIGURE 6 Distribution of the global residuals, *R*, for the ground motion suites selected using various scaling limits for hazard cases I to IV

the resultant quality of fit is generally in a similar level compared with group B. Thus, it seems that the use of excessive scaling in ground motion selection would not greatly improve the quality of fit.

3.4 | Comparison of non-SA IM distributions of the selected ground motion suites

Because of the complexity of seismic shaking, SA ordinates only cannot fully represent the ground motion characteristics. Thus, to comprehensively investigate the effect of scaling limits on the characteristics of selected ground motions, the distribution of non-SA IMs also needs to be examined. Some IMs commonly used in earthquake engineering are considered herein, including peak ground velocity (PGV), Arias intensity (Ia), significant duration ($Ds_{5\text{-}75}$), and the mean period (T_m). The definitions of these IMs, along with the GMPEs adopted, are listed in Table 4. It can be seen that the IMs employed can represent various aspects of ground motion characteristics (ie, peak velocity amplitude, cumulative energy, duration, and frequency content).

To obtain the statistical distribution of the non-SA IMs, the GCIM approach proposed by Bradley[7] is utilized. The conditional mean and standard deviation for these IMs can be similarly derived based on Equations (1) and (2). The

TABLE 4 Summary of the non–spectral acceleration intensity measures (IMs) and ground motion prediction equations (GMPEs) considered in this study

IM	Definition	GMPEs
PGV	Peak ground velocity	Campbell and Bozorgnia[27]
Ia	Arias intensity[28]	Foulser-Piggott and Stafford[29]
$Ds_{5\text{-}75}$	Significant duration (time interval between 5% and 75% of Ia)	Du and Wang[30]
T_m	The weighted average period in the Fourier spectrum[31]	Du[32]

GMPEs listed in Table 4 are used for estimating the statistical distribution of the IMs based on the target causal parameters. Several researchers have studied the empirical correlations of SA with the non-SA IMs,[33-36] which are utilized for obtaining the correlation coefficients between these IMs and SA at period T^*.

Figures 7 and 8 present the empirical CDFs of the non-SA IMs (ie, PGV, Ia, $Ds_{5\text{-}75}$, and T_m) of selected ground motion suites for hazard cases I and IV, respectively. The GCIM distributions of these IMs, as well as the Kolmogorov-Smirnov (KS) test bounds at 5% significance level, are also presented in these figures. Note that these IMs are not considered as "target" in the selection process, so it is not surprising that some empirical curves of these IMs (eg, Figure 7A and 8C) have a biased distribution (lie outside the KS bounds). Specifically, most empirical curves of Ia lie outside the KS bounds in Figure 8B, which is perhaps due to the incompatibility between the selected ground motion recordings and the GMPE employed. The ground motions are selected from the NGA-West2 database, whereas the GMPE for predicting Ia[29] was developed based on the original NGA-West1 database. For each hazard case, it can be seen that the ground

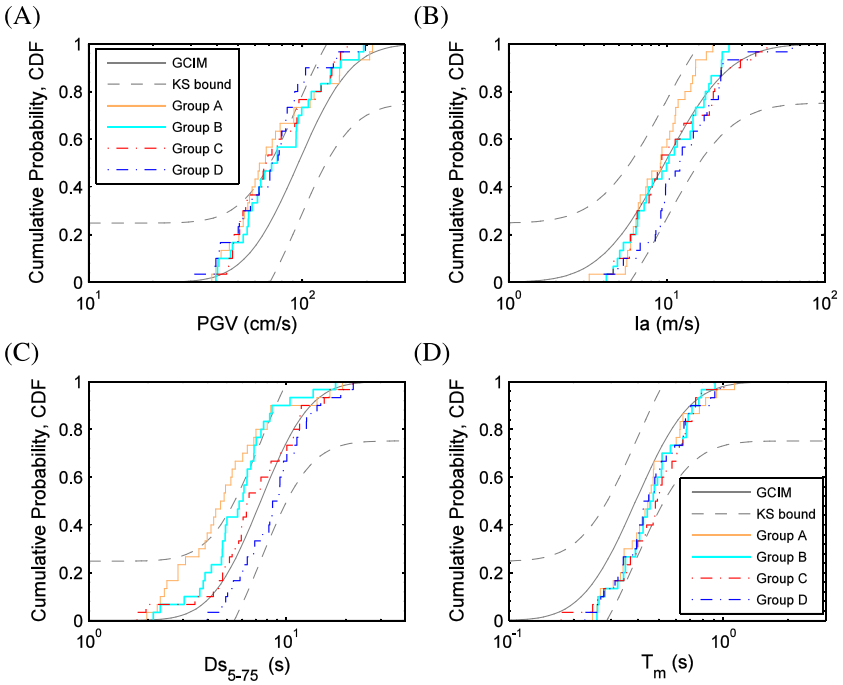

FIGURE 7 Empirical cumulative distribution functions (CDFs) of (A) PGV, (B) Ia, (C) $Ds_{5\text{-}75}$, and (D) T_m of the selected ground motions (groups A-D) for hazard case I. In these and the subsequent plots, the "GCIM" curve is obtained based on the GCIM methodology proposed by Bradley,[7] and the KS test bounds at 5% significance level of these IMs are shown in each plot

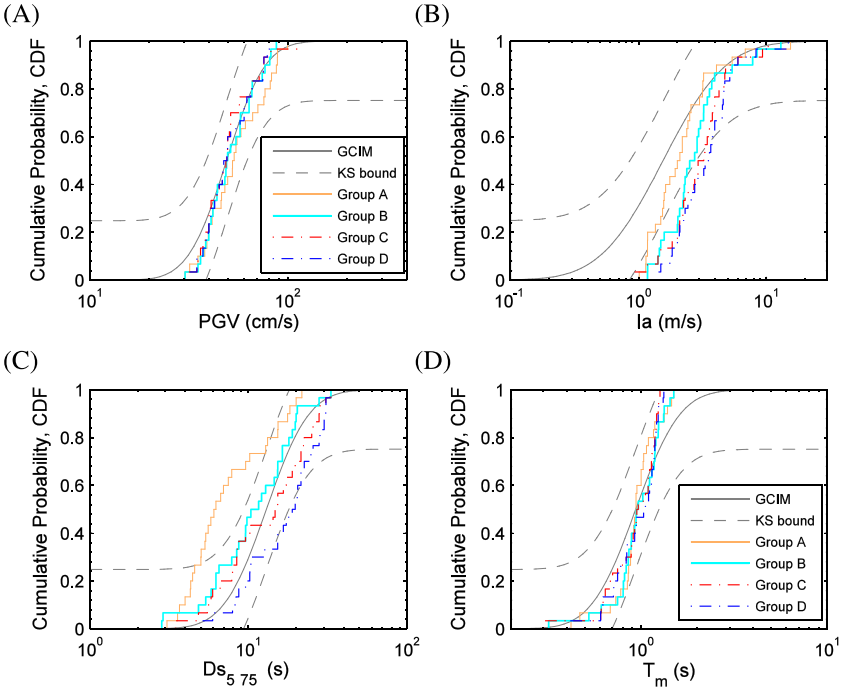

FIGURE 8 Empirical cumulative distribution functions (CDFs) of (A) PGV, (B) Ia, (C) $Ds_{5\text{-}75}$, and (D) T_m of the selected ground motions (groups A-D) for hazard case IV

motion groups selected using different scaling limits have a generally consistent distribution for PGV and T_m, while they have distinctively different distributions for Ia and $Ds_{5\text{-}75}$.

Figure 9 further compares the calculated geometric means of the IMs of selected ground motion suites for all hazard cases. For each hazard case, the geometric mean PGV and T_m values are in a similar range, whereas the geometric mean values of Ia and $Ds_{5\text{-}75}$ generally increase with increasing scaling limit (ie, from group A to group D).

Physical reasons regarding the observations above are explored. Scaling limit has a little influence on the distributions of PGV and T_m of the selected ground motions. This might be due to the fact that (a) PGV exhibits moderate and strong positive correlations with SA ordinates at short and moderate-to-long periods, respectively[34]; (b) both T_m and the shape of a response spectrum represent the frequency-content characteristic of a ground motion, so the magnitude of T_m is highly correlated with the spectral shape. Therefore, once the goodness of fit in terms of the target CS is guaranteed when selecting a ground motion suite, the statistical distributions of PGV and T_m can be, to a large extent, intrinsically constrained irrespective of the scaling limit assigned.

On the other hand, as scaling limit increases, the cumulative distributions of Ia and $Ds_{5\text{-}75}$ become generally larger. The effect of scale factors on the magnitude of non-SA IMs is different. For example, the magnitude of $Ds_{5\text{-}75}$ is independent of scale factors, whereas the magnitude of Ia is proportional to the square of the scale factor assigned (Ia increases by a factor of λ^2 if a scale factor λ is employed). Thus, applying an excessive scaling limit tends to result in ground motion suites with an enlarged distribution of Ia. The reason of the increase of $Ds_{5\text{-}75}$ is explained as follows. The use of a larger scaling limit leads to a ground motion suite consisting of more (originally) low-amplitude records. Note that the low-amplitude records are generally associated with relatively far rupture distance earthquake scenarios, which tend to result in long-duration ground motions.[30] Consequently, a ground motion suite selected using excessive scaling will possibly have an enlarged distribution of $Ds_{5\text{-}75}$. It is therefore evident that scaling limit consideration can have a significant influence on the cumulative and duration characteristics of selected ground motions.

4 | SEISMIC SLOPE SLIDING DISPLACEMENT ANALYSIS

4.1 | Simplified slope models

The effect of scaling limits on the characteristics of the selected ground motion suites has been thoroughly studied in the previous section. It is of interest in this section to estimate the dynamic performance of generic slopes, using ground motion suites selected with various scaling limits.

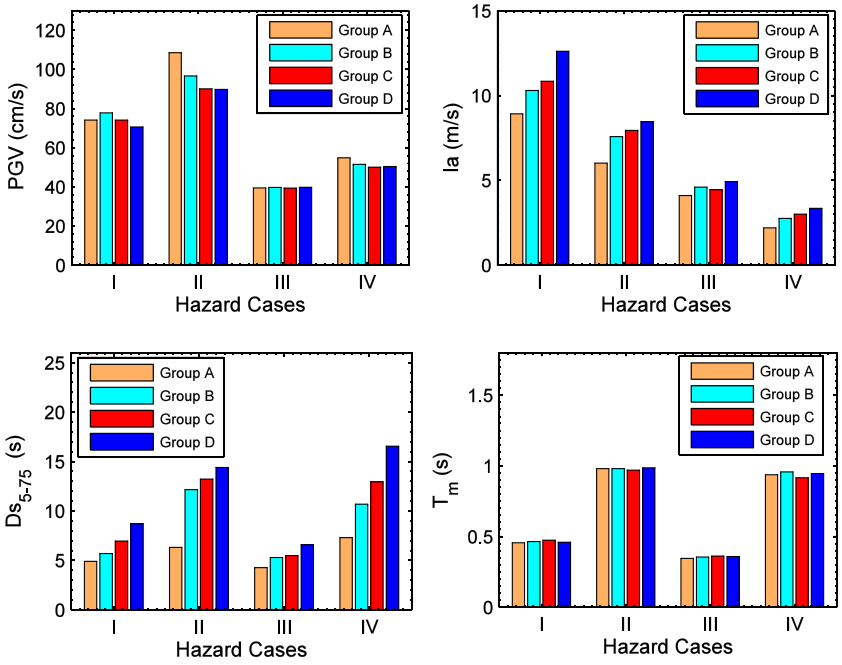

FIGURE 9 Distributions of the geometric mean values of PGV, Ia, $Ds_{5\text{-}75}$, and T_m of ground motion groups A to D for all hazard cases

Evaluation of the coseismic sliding displacement of slopes, earth dams, or embankments is an important topic in geotechnical earthquake engineering. Seismic sliding displacement analyses for flexible sliding masses are conducted herein based on an equivalent-linear coupled stick-slip sliding mass model.[37-39] In this model, the sliding mass is simplified as a generalized single-degree-of-freedom system governed by its first modal shape of vibration, and nonlinear soil properties are implemented using an equivalent-linear method. The detailed mathematical procedures of this model have been summarized in Wang.[40] The initial fundamental period (T_s) and yield acceleration (K_y) are used for characterizing the stiffness and dynamic strength of a sliding mass, respectively. T_s can be estimated by the following expression: $T_s = 4H/V_s$, where H and V_s denote the average height and average shear wave velocity of a potential sliding mass, respectively. Sliding initiates if the base acceleration exceeds K_y, and cumulative irreversible displacement can be calculated based on dynamic analysis. A demonstration of the potential sliding mass is illustrated in Figure 10.

Two kinds of potential sliding masses are considered, with T_s values of 0.2 and 1.0 second, respectively. The sliding masses were assigned as a constant unit weight of 18 kN/m^3, a plasticity index (PI) of 30, and a V_s value of 240 m/s. Nonlinear properties of soils were modeled using an equivalent-linear method, and the strain-dependent shear modulus reduction and material damping ratio curves proposed by Darendeli[41] were used. The K_y values considered are in the range of 0.05 to 0.2 g. Slope displacements are then calculated based on the combination of K_y and T_s using the ground motion suites selected in Section 3.

4.2 | Comparison of the calculated slope displacements using selected ground motion suites

The ground motion suites selected for hazard cases I, III ($T^* = 0.2$ s), and II, IV ($T^* = 1.0$ s) are used for computing the displacement of slopes with T_s values of 0.2 and 1.0 second, respectively. Figure 11A-D displays the comparisons of the empirical CDFs of the calculated displacements using ground motion groups A to D for $K_y = 0.05$ g for seismic hazard cases I to IV, respectively. It can be seen that in each plot, although the displacement distributions are broadly

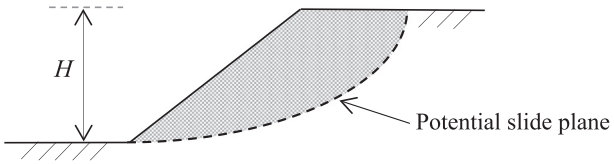

FIGURE 10 Demonstration of a potential sliding mass. In this study, H is assigned as 12 m ($T_s = 0.2$ s) and 60 m ($T_s = 1.0$ s), respectively

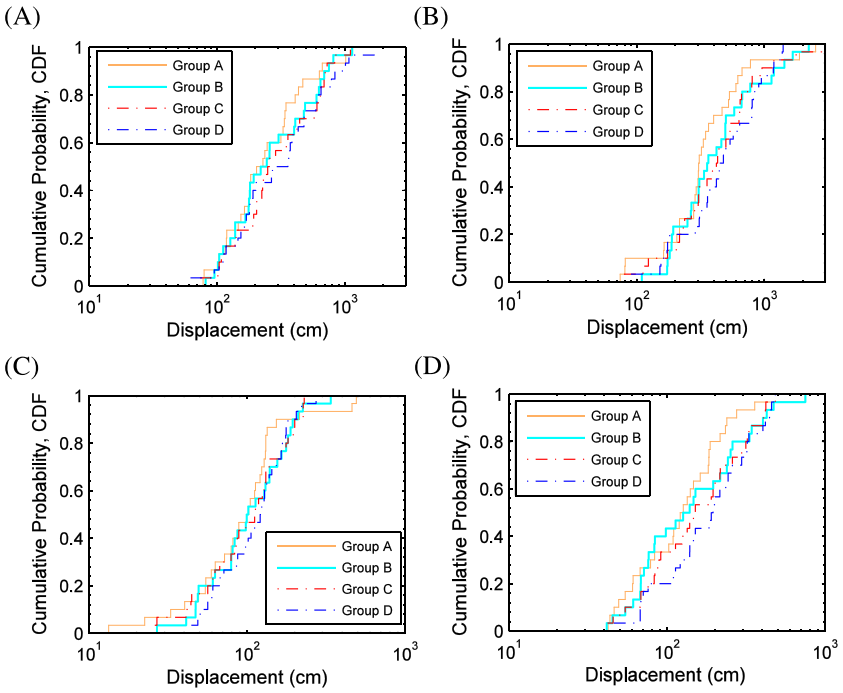

FIGURE 11 Empirical cumulative distribution functions (CDFs) of the calculated sliding displacements ($K_y = 0.05$ g) using ground motion groups A to D for hazard cases (A) I, (B) II, (C) III, and (D) IV, respectively

consistent, the displacements calculated using ground motion groups C and D (with excessive scaling limits) are generally larger than the other groups, especially compared with group A.

The calculated median displacements for these cases are compared in Figure 12. It can be observed that there is a clear increase in the median displacements with increasing scaling limit; the percentage increase estimated by group D, with respect to group B, is in the range of 20% to 50%. Such increase ratio is notable given the calculated standard deviations of the natural logarithm of displacements being about 0.7. As illustrated in Figures 3 and 4, the response spectra of the ground motion suites A to D for each hazard case are generally consistent, so the increase in the calculated displacements can be attributed to the different distributions of non-SA IMs, ie, Ia and $Ds_{5\text{-}75}$, as demonstrated in Figures 7 and 8. Previous studies[38,42] have reported a strong correlation between Ia and slope displacement, so the increasing trend of displacements might be mainly caused by the increase of Ia of selected ground motion suites.

These observations confirm that, using input motions selected based on different scaling limits indeed has an influence on the calculated displacements of sliding masses. Although the ground motion suites (groups A-D) have a similar representation of the target spectra, the displacements calculated using ground motions selected with a higher scaling limit are generally larger.

5 | STRUCTURAL DYNAMIC ANALYSIS

Two steel special moment frames, which are one-story, one-bay and three-story, three-bay structures, respectively, are further modeled and employed for dynamic analysis, using the ground motion suites selected with various scaling limits. They are modeled using OpenSees,[43] based on the two-story moment frame example posted by Dr Laura Eads (accessible via http://opensees.berkeley.edu/wiki/index.php). The steel frames have the following design features: (a) The nonlinear behavior is represented based on the concentrated plasticity concept; (b) the rotational behavior of the plastic regions is defined based on the Modified Ibarra Krawinkler Deterioration Model[44-46]; (c) the cyclic deterioration effect is neglected; (d) a leaning column is linked to the frame to denote P-delta effects. The schematics of the moment frames are illustrated in Figure 13. The frames are simulated using elastic elements with plastic hinges. The calculated fundamental periods of the two structures are 0.20 and 1.01 seconds, respectively.

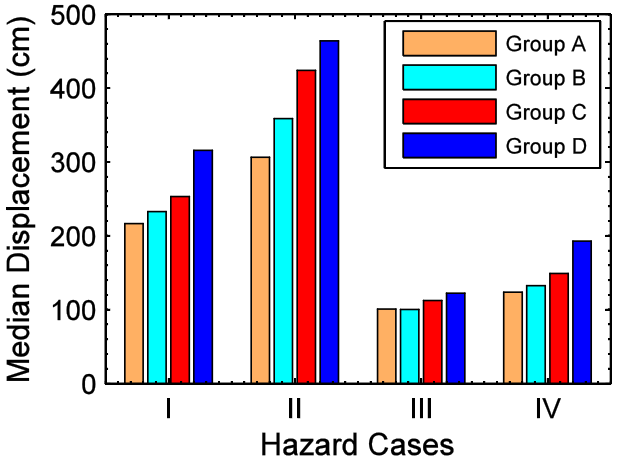

FIGURE 12 Distribution of the calculated median displacements using ground motion groups A to D for hazard cases I to IV

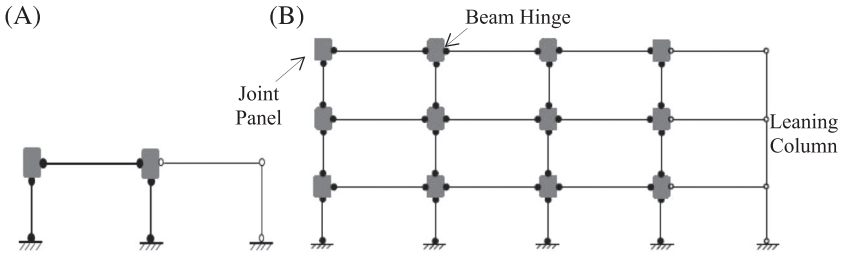

FIGURE 13 Schematic representation of (A) one-story, one-bay and (B) three-story, three-bay steel moment resisting frame models. The fundamental periods are 0.20 and 1.01 seconds, respectively

The ground motion suites for hazard cases I and II are used as input for dynamic analysis of steel frames with fundamental periods of 0.20 and 1.01 seconds, respectively. The maximum interstory drift ratio (MIDR) of all stories is adopted as the engineering demand parameter (EDP), and an unbounded increase in MIDR (eg, a threshold of 0.1 *rad*) can be regarded as structure collapse. Figure 14 compares the empirical CDFs of the calculated MIDRs using ground motion groups A to D for seismic hazard cases I and II, respectively. Although broadly consistent results can be observed for both plots, group D (with the largest scaling limit) exhibits the largest median MIDRs, about 10% and four times larger than those of group B for hazard cases I and II, respectively. Thus, similar to the observation in Section 4, ground motions selected based on excessive scaling would possibly yield overestimation of the calculated EDPs. Recent studies[15,47] have also demonstrated that ground motions with a biased distribution of Ia or $Ds_{5\text{-}75}$ can yield a systematic bias in dynamic responses of engineering systems. Therefore, ground motions selected using excessive scaling may introduce a bias in dynamic analysis, because of the inappropriate representation of the distribution of cumulative- and duration-based IMs.

Based on the results demonstrated in Sections 4 and 5, a scaling limit of 5 seems advisable when selecting ground motions for dynamic analysis, whereas the scaling limit should not exceed 10 to avoid excessive scaling (as well as subsequent bias in dynamic analysis).

6 | DISCUSSIONS

The results above indicate that the use of a small scaling limit in the CS-based ground motion selection degrades the goodness of fit regarding the target spectra, whereas the use of an excessive limit can yield a biased distribution with respect to some non-SA IMs. An additional analysis is then conducted to identify the "optimal" scaling limit in selecting ground motions for general applications. Eighteen scaling limits are considered, which are evenly spaced between 1.5 and 10. In addition to the soil site condition (V_{s30} = 360 m/s) previously used in cases I to IV, a soft rock site of V_{s30} = 760 m/s is also incorporated in this analysis. The number of records in a ground motion suite (N_{gm}) is set as 7, 15, and 30, respectively. Therefore, for the four hazard targets ($\overline{M}_w/\overline{R}_{rup}/\varepsilon$ shown in Table 2), a total of $4 \times 2 \times 3 \times 18 = 432$ ground motion selection analyses were conducted.

Figure 15A,B displays the calculated global residuals *R* with respect to scaling limits for the soil and rock site conditions, respectively. Again, the selection constraint on V_{s30} ($[0.5V_{s30}, 1.5V_{s30}]$) is applied to each case. In each plot, *R* decreases rapidly with increasing scaling limit at values smaller than 3, and it keeps almost constant in which the scaling limits are larger than 5. Therefore, a scaling limit in the range of 3 to 5 is generally recommended when selecting ground motions from the NGA-West2 database. Another observation is that, as the sample size N_{gm} increases, the variation of *R* versus scaling limit becomes more notable. This indicates that the impact of scaling limit will be more significant if a larger sample size is required in selecting ground motions.

The use of an excessive scaling limit in ground motion selection is not recommended, because it would not only increase the computational cost but also tend to result in the selected ground motions with a less desirable representation of the cumulative and duration characteristics. However, it might be an inevitable choice, for instance, if the available ground motion dataset is small. In such a case, selecting ground motions based on generalized IMs rather than SA ordinates only would be more suitable. Some cumulative- and duration-based IMs, such as Ia and $Ds_{5\text{-}75}$, need to be incorporated as "target" in the ground motion selection process, to provide additional constraints on the earthquake characteristics.

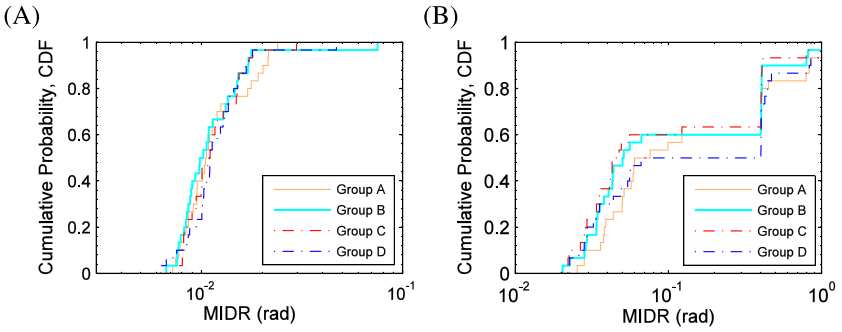

FIGURE 14 Empirical cumulative distribution functions (CDFs) of the calculated maximum interstory drift ratios (MIDRs) using ground motion groups A to D for the dynamic performance of (A) one-story, one-bay frame (hazard case I); (B) three-story, three-bay frame (hazard case II), respectively

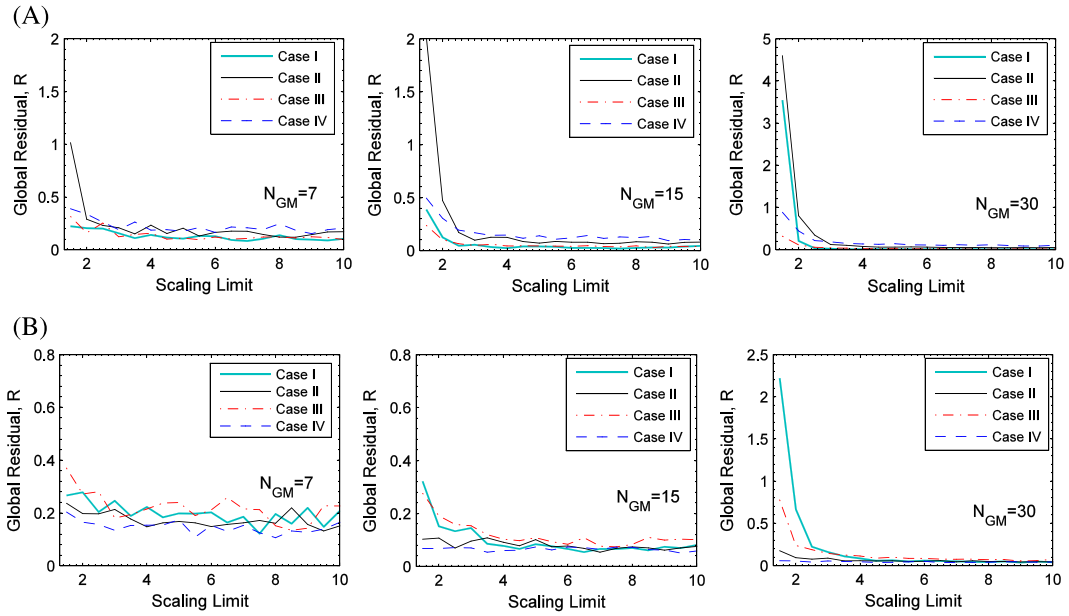

FIGURE 15 Calculated global residuals *R* with respect to scaling limits for hazard cases I to IV and different sample sizes for (A) soil site of V_{s30} = 360 m/s; (B) rock site of V_{s30} = 760 m/s

7 | CONCLUSIONS

This study comprehensively investigated the effect of scaling limits on CS-based ground motion selection. Sixteen ground motion suites were selected using four scaling limits (ie, 2, 5, 10, and 15) based on four seismic hazard cases in Western United States. It was observed that using the scaling limit of 2 yields the largest misfit regarding the target spectra, which is due to the fewest available ground motions under such a scaling restriction; the goodness of fit for ground motions selected using the other scaling limits is generally similar. Besides, the distributions of non-SA IMs of selected ground motion suites were compared. The IMs consist of PGV, Ia, $Ds_{5\text{-}75}$, and T_m. It was demonstrated that the change of a scaling limit does not noticeably influence the statistical distribution of PGV and T_m of selected ground motions, whereas it has a great influence on the distribution of Ia and $Ds_{5\text{-}75}$. The application of a larger scaling limit would, in general, lead to a ground motion suite with larger distributions of Ia and $Ds_{5\text{-}75}$, as a result of insufficient constraints on the cumulative and duration characteristics of ground motions selected.

The ground motion suites selected were then used as input for seismic slope displacement and structural analyses. Comparative results demonstrated that the choice of a scaling limit can influence the distribution of the calculated EDPs (ie, slope sliding displacement and MIDR); the median EDPs broadly increase as scaling limit increases. Therefore, ground motions selected with excessive scaling could likely introduce a bias in dynamic analysis of engineering systems, because of the exaggerated distributions of cumulative- and duration-based IMs of ground motions.

Finally, an additional analysis was conducted to find the "optimal" scaling limit in selecting ground motions from the NGA-West2 database. It was shown that a scaling limit of 3 to 5 is desirable to make a compromise between the goodness of fit with respect to the target and the computational cost. Thus, when selecting ground motions, the scaling limit of 3 to 5 is recommended for general use, with allowable adjustments for specific applications. For cases in which excessive scaling has to be applied, the use of the GCIM-based approach is recommended, in order to guarantee an appropriate representation of the non-SA IM distributions.

ACKNOWLEDGEMENTS

The authors acknowledge support from General Research Fund (grant no. 16204618) from Hong Kong Research Grants Council and Joint Research Fund for Overseas Chinese Scholars and Scholars in Hong Kong and Macao (grant no. 51828902) from National Natural Science Foundation of China. The authors thank anonymous reviewers for their helpful comments to improve this manuscript.

ORCID

Wenqi Du https://orcid.org/0000-0002-4392-6255
Gang Wang https://orcid.org/0000-0001-5237-8097

REFERENCES

1. CEN. Design of structures for earthquake resistance. Part 1: General rules, seismic actions and rules for buildings. EN 1998–1, European Committee for Standardization, Brussels, Belgium, 2004.
2. ASCE. (2016). Minimum design loads for buildings and other structures. ASCE/SEI 7-16, Reston, VA, 2016
3. Baker JW. Conditional mean spectrum: tool for ground-motion selection. *J Struct Eng*. 2011;137(3):322-331.
4. Jayaram N, Lin T, Baker JW. A computationally efficient ground-motion selection algorithm for matching a target response spectrum mean and variance. *Earthq Spectra*. 2011;27(3):797-815.
5. Kottke A, Rathje EM. A semi-automated procedure for selecting and scaling recorded earthquake motions for dynamic analysis. *Earthq Spectra*. 2008;24(4):911-932.
6. Atik L, Abrahamson N. An improved method for nonstationary spectral matching. *Earthq Spectra*. 2010;26(3):601-617.
7. Bradley BA. A generalized conditional intensity measure approach and holistic ground-motion selection. *Earthq Eng Struct Dyn*. 2010;39(12):1321-1342.
8. Katsanos EI, Sextos AG, Manolis GD. Selection of earthquake ground motion records: a state-of-the-art review from a structural engineering perspective. *Soil Dyn Earthq Eng*. 2010;30(4):157-169.
9. Wang G. A ground motion selection and modification method capturing response spectrum characteristics and variability of scenario earthquakes. *Soil Dyn Earthq Eng*. 2011;31(4):611-625.
10. Bradley BA. A ground motion selection algorithm based on the generalized conditional intensity measure approach. *Soil Dyn Earthq Eng*. 2012;40:48-61.
11. Lin T, Haselton CB, Baker JW. Conditional spectrum-based ground motion selection. Part I: hazard consistency for risk-based assessments. *Earthq Eng Struct Dyn*. 2013;42(12):1847-1865.
12. Bradley BA, Burks LS, Baker JW. Ground motion selection for simulation-based seismic hazard and structural reliability assessment. *Earthq Eng Struct Dyn*. 2015;44(13):2321-2340.
13. Tarbali K, Bradley BA. Ground motion selection for scenario ruptures using the generalised conditional intensity measure (GCIM) method. *Earthq Eng Struct Dyn*. 2015;44(10):1601-1621.
14. Wang G, Youngs R, Power M, Li Z. Design ground motion library (DGML): an interactive tool for selecting earthquake ground motions. *Earthq Spectra*. 2015;31(2):617-635.
15. Du W, Wang G. Ground motion selection for seismic slope displacement analysis using a generalized intensity measure distribution method. *Earthq Eng Struct Dyn*. 2018;47(5):1352-1359.
16. Beyer K, Bommer JJ. Selection and scaling of real accelerograms for bi-directional loading: a review of current practice and code provisions. *J Earthq Eng*. 2007;11(S1):13-45.
17. Hancock J, Bommer JJ, Stafford PJ. Numbers of scaled and matched accelerograms required for inelastic dynamic analyses. *Earthq Eng Struct Dyn*. 2008;37(14):1585-1607.
18. Kayhan AH, Korkmaz KA, Irfanoglu A. Selecting and scaling real ground motion records using harmony search algorithm. *Soil Dyn Earthq Eng*. 2011;31(7):941-953.
19. Watson-Lamprey J, Abrahamson N. Selection of ground motion time series and limits on scaling. *Soil Dyn Earthq Eng*. 2006;26(5):477-482.
20. Luco N, Bazzurro P. Does amplitude scaling of ground motion records result in biased nonlinear structural drift responses? *Earthq Eng Struct Dyn*. 2007;36(13):1813-1835.
21. Mehdizadeh M, Mackie KR, Nielson BG. Scaling bias and record selection for quantifying seismic structural demand. *J Struct Eng*. 2017;143(9):04017117.
22. Baker JW, Jayaram N. Correlation of spectral acceleration values from NGA ground motion models. *Earthq Spectra*. 2008;24(1):299-317.
23. USGS web tool. Available from: https://earthquake.usgs.gov/hazards/interactive/ [Accessed on February, 2018].
24. Lin T, Harmsen SC, Baker JW, Luco N. Conditional spectrum computation incorporating multiple causal earthquakes and ground-motion prediction models. *Bull Seismol Soc Am*. 2013;103(2A):1103-1116.
25. Tarbali K, Bradley BA. The effect of causal parameter bounds in PSHA-based ground motion selection. *Earthq Eng Struct Dyn*. 2016;45(9):1515-1535.
26. Ancheta TD, Darragh RB, Stewart JP, et al. NGA-West2 database. *Earthq Spectra*. 2014;30(3):989-1005.
27. Campbell KW, Bozorgnia Y. NGA-West2 ground motion model for the average horizontal components of PGA, PGV, and 5% damped linear acceleration response spectra. *Earthq Spectra*. 2014;30(3):1087-1115.

28. Arias A. In: Hansen RJ, ed. *A Measure of Earthquake Intensity. In: seismic design for nuclear power plants*. Cambridge, MA: MIT Press; 1970:438-483.
29. Foulser-Piggott R, Stafford PJ. A predictive model for Arias intensity at multiple sites and consideration of spatial correlations. *Earthq Eng Struct Dyn*. 2012;41(3):431-451.
30. Du W, Wang G. Prediction equations for ground-motion significant durations using the NGA-West2 database. *Bull Seismol Soc Am*. 2017;107(1):319-333.
31. Rathje EM, Abrahamson NA, Bray JD. Simplified frequency content estimates of earthquake ground motions. *J Geotech Geoenviron Eng*. 1998;124(2):150-159.
32. Du W. An empirical model for the mean period (T_m) of ground motions using the NGA-West2 database. *Bull Earthq Eng*. 2017;15(7):2673-2693.
33. Bradley BA. Correlation of significant duration with amplitude and cumulative intensity measures and its use in ground motion selection. *J Earthq Eng*. 2011;15(6):809-832.
34. Bradley BA. Empirical correlations between peak ground velocity and spectrum-based intensity measures. *Earthq Spectra*. 2012;28(1):17-35.
35. Bradley BA. Correlation of arias intensity with amplitude, duration and cumulative intensity measures. *Soil Dyn Earthq Eng*. 2015;78:89-98.
36. Du W. Empirical correlations of frequency content parameters of ground motions with other intensity measures. *J Earthq Eng*. 2019, in press;23:1-19. https://doi.org/10.1080/13632469.2017.1342303
37. Rathje EM, Bray JD. Nonlinear coupled seismic sliding analysis of earth structures. *J Geotech Geoenviron Eng*. 2000;126(11):1002-1014.
38. Bray JD, Travasarou T. Simplified procedure for estimating earthquake-induced deviatoric slope displacements. *J Geotech Geoenviron Eng*. 2007;133(4):381-392.
39. Du W, Wang G, Huang D. Evaluation of seismic slope displacements based on fully coupled sling mass analysis and NGA-West2 database. *J Geotech Geoenviron Eng ASCE*. 2018;144(8):06018006.
40. Wang G. Efficiency of scalar and vector intensity measures for seismic slope displacements. *Front Struct Civ Eng*. 2012;6(1):44-52.
41. Darendeli MB. Development of a new family of normalized modulus reduction and material damping curves. *Ph.D. thesis*. Austin, Texas: University of Texas at Austin, 2001.
42. Du W, Wang G. Fully probabilistic seismic displacement analysis of spatially distributed slopes using spatially correlated vector intensity measures. *Earthq Eng Struct Dyn*. 2014;43(5):661-679.
43. Mazzoni S, McKenna F, Scott MH, Fenves GL. OpenSees command language manual, Pacific Earthquake Engineering Research (PEER) Center, 2006.
44. Ibarra LF, Medina RA, Krawinkler H. Hysteretic models that incorporate strength and stiffness deterioration. *Earthq Eng Struct Dyn*. 2005;34(12):1489-1511.
45. Lignos DG, Krawinkler H. Sidesway collapse of deteriorating structural systems under seismic excitations. Technical report 172, The John A. Blume Earthquake Engineering Research Center, Department of Civil Engineering, Stanford University, Stanford, CA, 2009.
46. Lignos DG, Krawinkler H. Deterioration modeling of steel beams and columns in support to collapse prediction of steel moment frames. *ASCE J Struct Eng*. 2011;137(11):1291-1302.
47. Chandramohan R, Baker JW, Deierlein GG. Impact of hazard-consistent ground motion duration in structural collapse risk assessment. *Earthq Eng Struct Dyn*. 2016;45(8):1357-1379.

How to cite this article: Du W, Ning C-L, Wang G. The effect of amplitude scaling limits on conditional spectrum-based ground motion selection. *Earthquake Engng Struct Dyn*. 2019;48:1030–1044. https://doi.org/10.1002/eqe.3173